Water Resources Research / Volume 57, Issue 11 / e2021WR029704

Research Article | Open Access

Investigating the Effects of Land Use Change on Subsurface, Surface, and Atmospheric Branches of the Hydrologic Cycle in Central Argentina

Sujan Pal, Francina Dominguez, Pablo Bollatti, Steven P. Oncley, Yi Yang, Javier Alvarez, Carlos M. Garcia

First published: 20 October 2021
https://doi.org/10.1029/2021WR029704

Abstract

Since the 1970s, land cover in central Argentina has shifted away from perennial crops and grasses toward annual crops, largely soy. In this study, we use observations and modeling to understand how this shift in land use has affected the sub-surface, surface, and atmospheric fluxes of moisture and energy in a flat agricultural area. We analyze the flux tower data from a paired site at Marcos Juarez in central Argentina during the period of the RELAMPAGO field campaign (2018–2019). When compared to perennial alfalfa, the observations over soy show lower evapotranspiration (ET) and specific humidity, higher sensible heat, higher outgoing shortwave radiation, and soil temperature. Water table (WT) depth is shallower below the soy than the alfalfa sites. To better understand the long-term temporal behavior from 1970s to present, the Budyko framework is used to show that the trends in ET cannot be explained by climate variables alone. We then use the Noah-MP land surface model calibrated at both soy and alfalfa sites. Long-term simulations of the calibrated model suggests that ~95% of precipitation is evaporated in the alfalfa site with negligible recharge and runoff. Contrarily in the case of soy, ET is about 68% of precipitation, leaving nearly 28% for recharge and 4% for runoff. Observed increases in streamflow and decreases in WT depth over time are likely linked to shifts in land cover. Furthermore, the partitioning of net radiation shifts from latent heat to sensible heat resulting in a 250% increase in Bowen ratio (from 0.2 to 0.7).

1 Introduction

During the 21st century, Argentina has experienced one of the fastest agricultural expansion rates in the planet (Baldi & Paruelo, 2008; Graesser et al., 2015). In many Argentinian regions the past 60 years have seen a shift in agricultural production from one that had primarily perennial crops for livestock and grasses to one based on annual crops, largely dominated by soy, with confinement of livestock into feedlots. These changes came about due technological advances in agricultural production such as the introduction of transgenic varieties, no-till farming, and crop rotation which dramatically increased crop productivity in the region (Paruelo et al., 2005). Global economic shifts such as the increasing demand of soy-based and corn-based biofuels made it economically attractive for farmers to shift to soy and corn. As a result, in two decades (1995/96 to 2014/15), the cultivated area in regions such as Cordoba increased by 229%. Soy now dominates the landscape in the province of Cordoba accounting for nearly 60% of crops.

How can these dramatic changes in land use affect the hydrologic cycle? Some effects could parallel those of other regions of the globe that have experienced similar land-use shifts, such as the Midwestern United States. In the US central region, European settlers arrived in the early to mid-19th century and by 1900 agriculture had become the dominant land use type, replacing the native grasses and forests of the region (Yaeger et al., 2013). Perennial and sod vegetation gave way to intensive corn and/or soybean crops with shorter summer growing seasons, which led to a decrease in evapotranspiration (ET). Decreased ET implied that more precipitation was going into groundwater recharge and routed into streams as baseflow (Zhang & Schilling, 2006). Several studies have attributed increased baseflow in the region to changes in land surface characteristics (Schilling et al., 2008, 2010; Xu et al., 2013; Zhang & Schilling, 2006).

The plains of the Pampas-Chaco in Argentina are flatter than their North American counterparts. They are sometimes referred to as hyperplanes, because their slopes are less than 0.1%, their drainage systems are poorly developed, and ET dominates the water balance (Jobbagy et al., 2008). Rodriguez et al. (2020) identified transpiration as the primary component of the water budget, followed by ET and interception, for dry forests and crops in the region of San Luis, Argentina. In general, their modeling results showed that water fluxes here are strongly controlled by the vegetation cover. Giménez et al. (2020) illustrated that changes in land cover from dry forests to crop reduced ET and increased intensity of deep drainage. Measurements and remote-sensing estimates in Argentina show that compared to annual crops, perennial crops such as alfalfa have deeper roots and year-round transpiration of more than 1,000 mm/year compared to about 680 mm/year for single summer crops (Nosetto et al., 2015). Soil moisture (SM) is usually higher, and the water table (WT) depth is closer to the surface below annual single summer crops than in areas where perennial alfalfa is grown (Nosetto et al., 2012). At inter-annual timescales, the balance between precipitation and ET dictates WT fluctuations, whereas crop choice can be a relevant control of WT at intra-annual or seasonal timescale (Mercau et al., 2015; Zellner et al., 2020). In addition, lateral transport of water, driven by hydraulic gradients develops

due to contrasting water consumption of different vegetation types (Mercau et al., 2015). One of the important consequences of changes in WT is related to flooding, as groundwater level is intimately related to the flooded area in the region (Aragón et al., 2010; Viglizzo et al., 2009). During periods of excess rains, the WT can reach the surface and cause "slow" floods that affect the region for several years (Kuppel et al., 2015). In fact, a modeling study by Lee et al. (2018) linked the increasing discharge of Parana river to land cover change using a terrestrial biosphere model.

Very few studies have relied on eddy covariance data in this region due to limited in-situ measurements. A. G. García et al. (2017) provided estimates of CO_2 and water vapor fluxes, using eddy covariance measurements, in a dry forest of central Argentina. They identified that the dry forest is a net sink of carbon, and that ET is the dominant vapor flux. In another study, Nosetto et al. (2020) compared the temporal patterns of CO_2 and water vapor fluxes of native dry forests and pastures at two different locations to show comparatively higher ET in the forests, primarily due to increased evaporating surface causing higher intercepted water. Long-term ground WT depth records are also limited in this region. Jobbággy et al. (2020) illustrated that unsaturated-saturated contact zone is a critical and dynamic hub of water partition using observed WT depth analysis at different vegetation. Clearly, this region shows strong interactions between land cover and terrestrial hydrology. However, there have not yet been any paired hydrometeorological observations of eddy-covariance estimates in the region, especially to understand how transient changes in land cover affect the partitioning of moisture and energy. Furthermore, the link between these differences and long-term trends in WT depth, hydrologic and atmospheric fluxes has not been established.

This study focuses on the regions surrounding Marcos Juarez, a town located in the Carcarañá river basin in the Pampas region of Argentina, in central-southeast of Cordoba province. This region has experienced a dramatic transformation from mostly perennial grasses and alfalfa to annual (mostly soybean) cultivation and is representative of the land-use changes in the region as a whole. Critically, the Argentinian National Institute for Agricultural Technology (INTA, for its acronym in Spanish) has an experimental alfalfa site and several soy sites in this location. Alfalfa is a perennial crop with characteristics similar to those that would have dominated the landscape in the 1970s, and soy crops are representative of the region at present. In addition, INTA has long-term WT depth observations (see Sections 2.1 and 3.1). We deployed two eddy covariance towers within the INTA site as part of the RELAMPAGO (Remote Sensing of Electrification, Lightning and Mesoscale/Microscale Processes with Adaptive Ground Observations) field campaign which took place in west-central Argentina (Nesbitt et al., 2016; Pal et al., 2021). The RELAMPAGO project consisted of an Extended Hydrometeorology Observing Period (EHOP) from 1 June 1, 2018 to April 30, 2019. One of the goals of the EHOP is to understand how changes in land cover have affected the partitioning of rainfall between infiltration/runoff and impacted the residence times of SM and groundwater in the Carcarañá Basin's terrestrial system. As part

of the EHOP, the hydrometeorology team of RELAMPAGO installed 30 meteorological stations, including seven eddy covariance towers. The work we present in this manuscript is based on the two eddy covariance towers located within the INTA experimental site in Marcos Juarez, Argentina.

In this study, we use the combined analysis of eddy covariance observations and land surface modeling to understand the potential effects of large-scale changes in land cover on the hydrology of the region. The specific goals of this manuscript are (a) to quantify the differences in energy and moisture fluxes between soy and alfalfa using high-resolution intra daily eddy covariance observations obtained from two RELAMPAGO flux towers, and (b) to use an idealized modeling framework to understand the potential changes in surface, subsurface, and atmospheric hydrology due to the gradual shift from perennial to annual crops. The results from this study can be used to interpret long-term ET estimates in this region, which are also useful for INTA. Critically, the results from this study have implications for interpreting changes in WT depth based on land cover type and climate variability (such as El Niño and La Niña conditions). The manuscript is organized as follows: in Section 2, the description of observed data, model specifications, and the experimental design are discussed. In Section 3, the results are discussed and finally, the conclusions are summarized in Section 4. Additional information is provided in Supporting Information S1.

2 Materials and Methods

2.1 Long-Term Observations

Long-term measurements (1970–2020) of annual mean WT depth, precipitation, and temperature were obtained from the agrometeorological station of the INTA Marcos Juárez (62.085°W, 32.725°S, Figures 1a and 1b). The region is currently dominated by crops, mainly soy. Annual runoff measurements from 1980 to 2020 were obtained from the streamflow station at Andino (Figure 1c). The Carcarañá river drains an area of ~40,000 km^2 at Andino (60.87°W, 32.67°S), which has long-term daily discharge information (available from https://www.argentina.gob.ar/obras-publicas/hidricas/base-de-datos-hidrologica-integrada). As such, Andino is downstream of Marcos Juarez as well as most of the Carcarañá river basin. Total streamflow at Andino was separated into baseflow and surface flow using the Web-based Hydrograph Analysis Tool (WHAT) recursive digital filter method (Eckhardt, 2012). Throughout the text, significance is assessed using the Mann Kendall trend test at a 95% significance level. The Sequential Mann Kendall test (Modarres & Sarhadi, 2009; Sneyers, 1990) was used to detect breakpoints in discharge (see Figure S1 in Supporting Information S1). Long-term record of land-use data was obtained from INTA Marcos Juarez, which indicates a gradual shift of land use from perennial crops to annual crops (Figure 2).

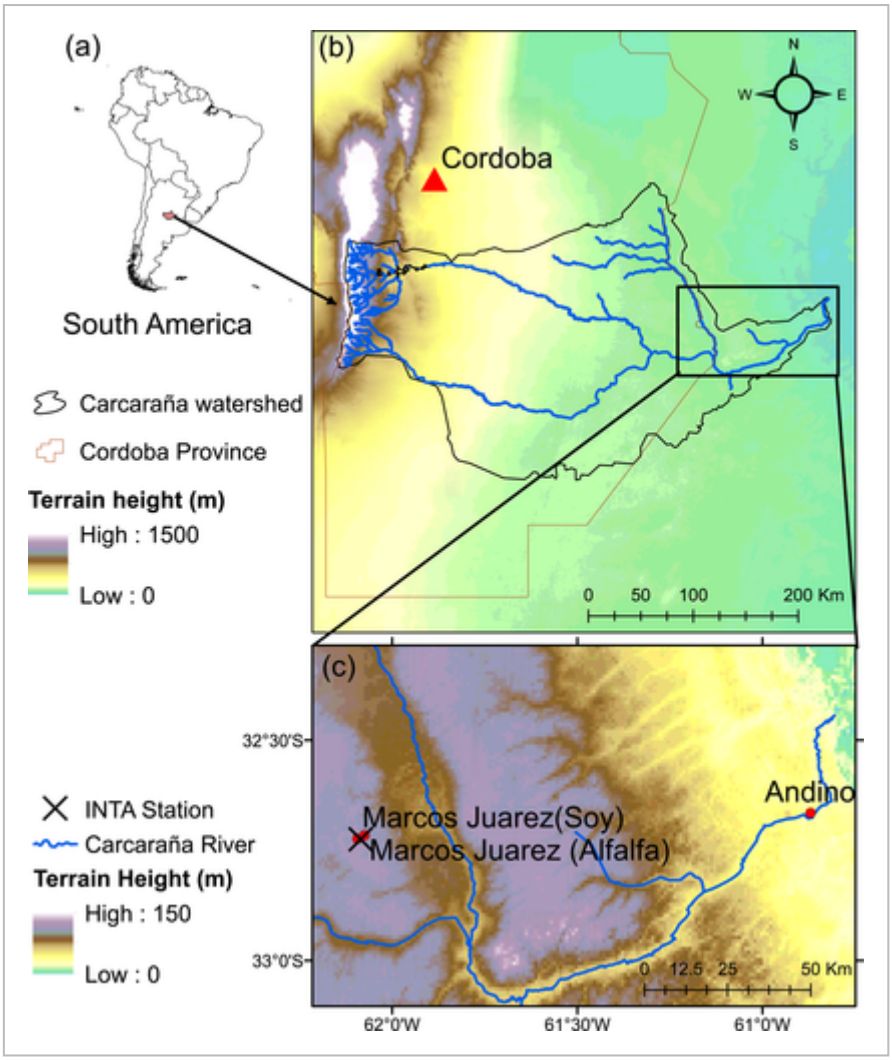

Figure 1

Open in figure viewer | PowerPoint

(a) Location of Carcarañá river basin in Argentina. (b) Elevation (m) and drainage network of the basin. (c) Location of Marcos Juarez (paired sites), INTA agrometeorological station and Andino (streamflow measurement location) within the watershed.

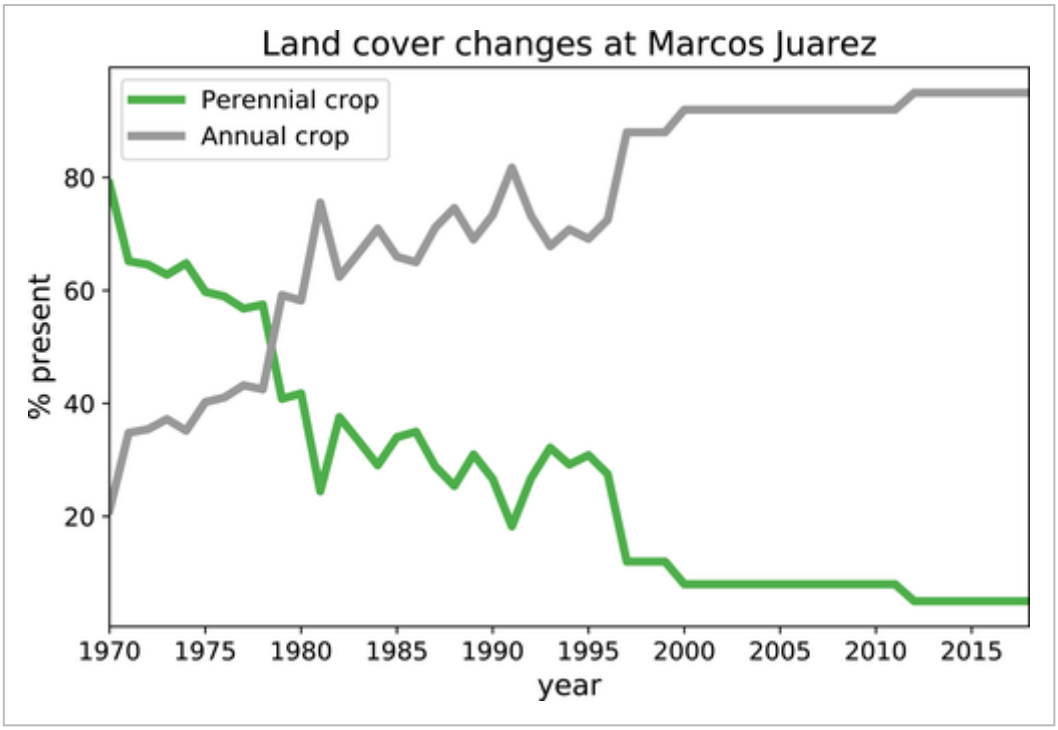

Figure 2

Open in figure viewer | PowerPoint

Time evolution of land use in Marcos Juarez.

2.2 Budyko Analysis

The Budyko framework has been extensively used in the literature to separate possible effects of climate and land cover change on hydro-climatological variables (Jaramillo et al., 2013; Levi et al., 2015; Xiong et al., 2020). To understand the possible climate-driven changes of hydroclimatic conditions at Marcos Juarez, actual ET (AET) was calculated according to two different methods (M1 and M2) following Levi et al. (2015). In M1, annual AET (AET_{wb}) was computed based on water balance, following Equation 1.

$$AET_{wb} = P - R - \Delta S \quad (1)$$

where P = annual precipitation, R = annual runoff, ΔS = annual change in storage. For our case of site-level analysis, considering unit area, change in storage was calculated from the change in WT depth and an approximate specific yield of the unconfined aquifer in the area (following Varni et al. [2013]). In M2, we calculated two climate based AET estimates, AET_{clim1} and AET_{clim2} computed with Budyko (1974) and Turc (1954), following Equations 2 and 3, respectively. Potential evapotranspiration (PET) was obtained from Langbein (1949), where T = mean annual temperature in °C. Two different equations were considered for M2 to account for potential uncertainty in the empirical methods.

$$\mathrm{AET}_{\mathrm{clim1}} = \frac{P}{\sqrt{0.9 + \frac{P^2}{\mathrm{PET}^2}}} \tag{2}$$

$$\mathrm{AET}_{\mathrm{clim\,2}} = P\left(1 - e^{\frac{-\mathrm{PET}}{P}}\right) \tag{3}$$

where

$$\mathrm{PET} = 325 + 21T + 0.9T^2 \tag{4}$$

2.3 RELAMPAGO 10-Month Observations

To understand the effects of different land-use types on the fluxes of energy, moisture, and momentum along the subsurface-surface and atmosphere continuum, the RELAMPAGO Hydrometeorology team installed two eddy covariance towers within the INTA experimental station in Marcos Juarez (Figure 1c). One of the towers was located within an alfalfa test plot (62.075°W, 32.71617°S), while the other one was located in a soy site (62.085°W, 32.725°'S; Figure 1c).

RELAMPAGO surface flux measurements were made by the Integrated Surface Flux System (ISFS) (https://www.eol.ucar.edu/content/isfs-operations-relampago) maintained by the National Center for Atmospheric Research (NCAR) Earth Observing Laboratory (EOL). Campbell Scientific 3-D sonic anemometers (CSAT3A) and open path H_2O/CO_2 gas analyzers (EC150) were used to measure sensible and latent heat fluxes (net ET) directly using the eddy-covariance (EC) method. The installation height of the EC system was 6 m at the soy site and 3 m at the alfalfa site. Maximum height of soy and alfalfa canopies were 1.18 and 1 m, respectively. We used a two-dimensional parameterization for flux footprint prediction based on 30-min data from the entire period to calculate the representative area for flux measurements at each site (FFPonline tool, Kljun et al., 2015). Based on this analysis, 80% of the daytime representative area was within 350 m of the soy site and 60 m of the alfalfa site. The flux footprint analysis is shown in Figure S2 of Supporting Information S1. The data were corrected for spatial separation between the anemometer and gas analyzer paths, for the

response of the anemometer acoustic temperature to both temperature and water vapor, and for the WPL density effect using the equations used by Oncley et al. (2007). To complete observations of the surface energy balance, the four radiation components were measured by a Hukseflux integrated radiometer (NR01) and the soil heat flux at the surface by a REBS heat flux plate at 5 cm depth, corrected for heat storage using a custom 4-level temperature profile sensor and a Hukseflux heat capacity sensor (TP01). Residuals in the energy balance averaged 17% for these two sites over the entire RELAMPAGO observation period, which is not atypical. Decagon SM sensors (EC5) also were installed at 5 cm depth and adjusted for biases of 12% and 13% vol, for the two sites, based on manual gravimetric observations taken several times during the study.

For this study, we analyze SM, sensible and latent heat fluxes (SHF and LHF, measured by the EC method), specific humidity (SH), outgoing shortwave radiation (OSR), soil temperature (ST), 2-m temperature (T2m), momentum in zonal and meridional direction (U-momentum and V-momentum), and incoming shortwave radiation (ISR). The flux tower measurements were available from June 1, 2018 to April 1, 2019. However, good quality SM data was only available from November 2018 to March 2019. Continuous groundwater measurements were obtained in the soy and alfalfa sites from both automated sensors and manual extraction by INTA and data were available from July 2018 to May 2019.

Our observations include the full crop planting-harvesting cycle. In Argentina, soy planting begins in September–October and planting ends in November, during the months of austral spring. December–February is the growing season (austral summer), and harvesting begins in March. Harvesting is completed by April–May. During the austral winter months, cover crops are also planted sometimes to improve soil fertility and quality. During the 2018–2019 season, a rye cover crop was planted before the soy crop in Marcos Juarez.

2.4 Land Surface Modeling With Noah-MP

Land surface models compute the exchanges of water, heat, radiation, and momentum between the land and atmosphere (Sellers et al., 1997; Zheng et al., 2019). In this study, we use the Noah LSM (Chen & Dudhia, 2001) with multi-parameterization options (Noah-MP; Niu et al., 2011) run in a column (one-dimensional in the horizontal direction) configuration. Noah-MP calculates energy, water, and carbon dioxide fluxes between the biosphere and the atmosphere for different vegetation types, with closed energy budget and coupled water cycle. It has been previously implemented to investigate problems related to hydrologic cycle of South America in standalone mode (Martinez et al., 2016a) and coupled with WRF (Martinez et al., 2016b; Sörensson & Berbery, 2015) or WRF-Hydro (Pal et al., 2021).

2.4.1 Model Configuration

We use the Noah-MP land surface model in “offline” mode with a groundwater scheme (Figure S3a in Supporting Information S1; Niu et al., 2007) to better understand the physical processes in the two sites with different vegetation and evaluate these processes for periods

in the past when we do not have observations. The Ball-Berry scheme was chosen for modeling stomatal resistance. Other parameterizations of Noah-MP were left as default; such as Monin-Obukhov scheme for surface layer drag, Jordan scheme for partitioning precipitation into rainfall and snowfall, and so on (Niu et al., 2011). We do not analyze carbon fluxes in this study, so the carbon and dynamic vegetation module was not used. Furthermore, we define leaf area index (LAI) and rooting depth (RD) climatology in the model and calibrate other vegetation-related parameters. We did not account for long-term changes in atmospheric CO_2 as it is kept constant at 375 ppm. Our tests showed the minimal effect of changing CO_2 in our simulations (not shown). In the model, vegetation is represented by generic plant functional types, so the model needs to be calibrated regionally for best results. To better represent the soil state and ground water-SM interaction, we modified the model soil column to have 14 layers (Table S1) extending from the surface to 4 m below (following Miguez-Macho and Fan [2012] and Martinez et al. [2016a]) as the default Noah-MP has only 2 m deep soil column (with 4 layers).

The model is run with prescribed atmospheric conditions from Global Land Data Assimilation System (GLDAS; Rodell et al., 2004) extracted for Marcos Juarez (nearest grid point from GLDAS). First, we performed two independent experiments named “Noah-MP SOY” and “Noah-MP ALFALFA” where the model configuration remains unchanged except for the vegetation parameters in the model. The vegetation parameters that varied depending on the type of crop were (a) LAI, (b) RD, (c) maximum carboxylation rate (VMAX) in the Farquhar photosynthesis model (Farquhar et al., 1980), (d) the slope parameter (MP), and (e) the intercept parameter (BP) in the Ball-Berry stomatal conductance model (Ball et al., 1987). VMAX, BP, and MP control the ET by controlling the stomatal resistance ($r_{s,i}$) following Equation 5.

$$\frac{1}{r_{s,i}} = MP\frac{A}{c_{air}}\frac{e_{air}}{e_{sat}\left(T_v\right)}P_{air} + BP \tag{5}$$

where “A” is photosynthesis rates per unit LAI of leaves, which is controlled by VMAX. C_{air} is the CO_2 concentration at leaf surface, P_{air} is the surface air pressure. E_{air} and e_{sat} are vapor pressure at leaf surface and saturation vapor pressure at leaf surface temperature, respectively. Simulated ET is highly sensitive to these parameters of Noah-MP (Cuntz et al., 2016). Other vegetation parameters (e.g., leaf reflectivity, stem reflectivity, vegetation height, height of lower canopy bound, etc.) for the Noah-MP ALFALFA and Noah-MP SOY simulations were kept as default Noah-MP values of “Grasslands” and “Croplands” from modified IGBP MODIS 20-category vegetation, respectively. The soil type was taken as silty clay loam for both sites.

The climatology of LAI and RD for the two vegetation types were obtained from literature (Figure 2 of P. E. García et al. [2017]). Alfalfa grows during the whole year and has a deeper root system (3.5 m), while soy crops occupy the field only 4–5 months. In Noah-MP, we provided the root depth monthly climatology and prescribed monthly LAI climatology (Figures S3b and S3c in Supporting Information S1) from P. E. García et al. (2017). As such, we did not use dynamic root or dynamic vegetation calculations. There are some remotely sensed LAI products (e.g., MODIS) available in this region providing estimates of combined LAI values from several different vegetation types within a grid cell, however, they do not represent the LAI climatology of these two specific vegetation types (see Figure S4 in Supporting Information S1). For this reason, we relied on the LAI estimates reported in the literature for the sensitivity experiments. MODIS LAI estimates are considered for the uncertainty experiments (Section 2.4.4).

The two short-term simulations Noah-MP ALFALFA and Noah-MP SOY were performed to calibrate and validate the model at the two sites (see Sections 2.4.2 and 3.3). The complete list of modeling experiments is presented in Table 1. Using the calibrated model (see Section 2.4.2) we performed two long-term simulations for 100% alfalfa and 100% soy conditions for the period January 1970 to December 2018 (Noah-MP ALFALFA LT and Noah-MP SOY LT, respectively in Table 1). The calibrated parameters for the two vegetation types are used in the long-term simulations, and the GLDAS forcing for 1970–2018 is used to capture the interannual variability of the model outputs. These simulations provide components of the annual water budget in the two different vegetation scenarios. It is important to highlight that these two scenarios are the two extremes of land use, and the actual transient land use would fall somewhere in between. However, this kind of idealized experiment helps us to understand the largest possible extent of transformation in hydrology due to land-use change in this region. In our modeling experiment, we do not take into account the effect of lateral flow (which might be generated by heterogeneous land cover) at inter-annual time scale. We spin up the model for 40 years for both scenarios and use the final SM and WT depth as the initial condition for the analyzed simulations.

Table 1. List of Experiments Performed in This Study

Name of simulation	Simulation period	Vegetation	Forcing	Purpose
Noah-MP ALFALFA	June 1, 2018 to April 1, 2019	100% alfalfa	GLDAS	Calibration and validation
Noah-MP SOY	June 1, 2018 to April 1, 2019	100% soy	GLDAS	Calibration and validation
Noah-MP ALFALFA LT	January 1, 1970 to December 31, 2018	100% alfalfa	GLDAS	Long term estimates of water budget and surface fluxes

Name of simulation	Simulation period	Vegetation	Forcing	Purpose
Noah-MP SOY LT	January 1, 1970 to December 31, 2018	100% soy	GLDAS	Long term estimates of water budget and surface fluxes

2.4.2 Model Calibration

In Noah-MP, ET is most sensitive to the vegetation parameters VMAX, BP, and MP (Cuntz et al., 2016). So, these parameters were obtained by calibration of the model based on RELAMPAGO flux tower observations of daily LHF at both sites. All other parameters of the model were kept constant as the default configuration (Section 2.4.1). The calibration was performed in a shuffle complex evolution method (Duan et al., 1993) minimizing the root mean square error (RMSE) of daily LHF data. Python SPOTPY package (Houska et al., 2015) was used to carry out the calibration. Using this method, we can make realistic estimates of land surface variables at these two sites using Noah-MP (which previously had default generic crop parameters). The model was calibrated separately with respect to daily LHF data at both sites to obtain the above-mentioned vegetation parameters. About 100 iterations for each site were carried out as RMSE improvements were insignificant in both scenarios with more iterations. It is worth remembering here that our main goal from these modeling exercises is to obtain realistic water and energy balances for these two types of vegetation. LHF is a major part of both energy and water balance (as ET). Hence, we preferred to calibrate the model based on the common link (ET) of these two budget equations. The model was validated using other variables during the same time period (June 1, 2018 to April 1, 2019).

2.4.3 Transient Analysis

To estimate the transient moisture and energy fluxes, we used the yearly land cover for the region as shown in Figure 2. It is important to highlight that, in reality, land cover in the region changed from mostly grasses and perennial crops like alfalfa, to a mixture of annual crops including soy, corn, wheat, and other crops. Our simulations greatly simplify this complexity by assuming that the land cover is composed of a mixture of only alfalfa and soy. Furthermore, we do not account for the use of cover crops, despite the fact that these are sometimes used during the winter months. Hence, the experiments will provide a first-order idea of the transient fluxes but will likely not reflect the actual historical conditions. The annual values were calculated based on a weighted “tile” approach commonly used in land surface models. For example, *i*th year values of latent heat flux (LH_i) were calculated following Equation 6.

$$LH_i = \frac{LH_{alfalfa} * (\%\, alfalfa) + LH_{soy} * (\%\, soy)}{100} \quad (6)$$

This method was followed for other fluxes as well.

2.4.4 Uncertainty Quantification

In this idealized modeling, uncertainty in the model results may originate from several factors—model forcing, model parameters, vegetation parameters. Among these, LAI is perhaps the most uncertain parameter due to the lack of direct measurements and the use of cover crops. To understand the range of combined uncertainty originating from a subset of these factors in the long-term simulations, we consider ensemble simulations with different extreme conditions. Cover crop LAI during the months of April–October was varied between 0 and 1. Soil parameter SMCMAX was varied from 0.38 to 0.47. Princeton Global Forcing was considered in addition to GLDAS (Figure S5 in Supporting Information S1). The extreme results from these additional simulations are shown as "uncertainty bounds" across original GLDAS deterministic simulations. It is important to highlight that this quantification is not comprehensive and limited to uncertainty originating from LAI, soil, and model forcing. Nonetheless, it provides a first-order estimate and motivates us to improve the quality and quantity of future observations to reduce uncertainties in model estimates.

3 Results

3.1 Analysis of Long-Term Data

In 1970, the WT was nearly 11 m deep, however, there has been a steady rise (statistically significant decreasing trend) of the WT and now it is approximately 2 m below ground at Marcos Juarez (Figure 3a). This trend does not seem to be related to climatic variables, for example, precipitation and temperature. Annual mean precipitation shows a slight statistically non-significant decreasing trend (Figure 3b) and annual mean temperature shows a statistically significant increasing trend (Figure 3c). Streamflow at Andino also has a statistically significant increasing trend, especially after 2000 (Figure 4). The increasing trend in total flow is result of both increased baseflow (statistically significant trend) and surface flow (statistically non-significant trend, Figure 4a). The year 2000 was found to be a year of change-point of trend (sequential Man-Kendall test, Figure S1 in Supporting Information S1). After 2000, baseflow has increased in the months of March and April; whereas surface flow has increased remarkably in February, March, and October (Figure 4b). It is important to clarify that the drainage area of Andino is the entire Carcarañá basin, and hence the change in discharge represents an accumulated effect on the entire watershed and not only Marcos

Juarez. It is clear that the combined effect of surface runoff and baseflow has resulted in the overall increase in streamflow at the Andino gauging station (Figures 4b–4d).

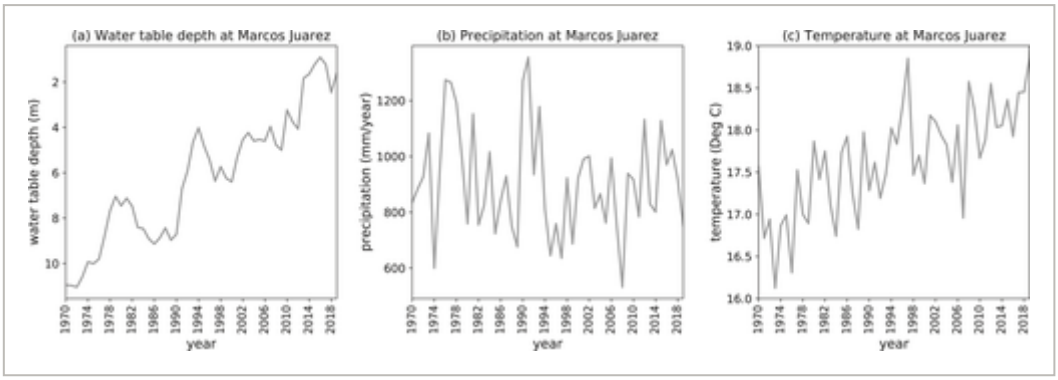

Figure 3

Open in figure viewer | PowerPoint

Long-term time series of annual mean (a) water table (WT) depth, (b) precipitation, and (c) temperature at Marcos Juarez based on the Agrometeorological Station of the INTA Marcos Juárez and manual WT depth observations.

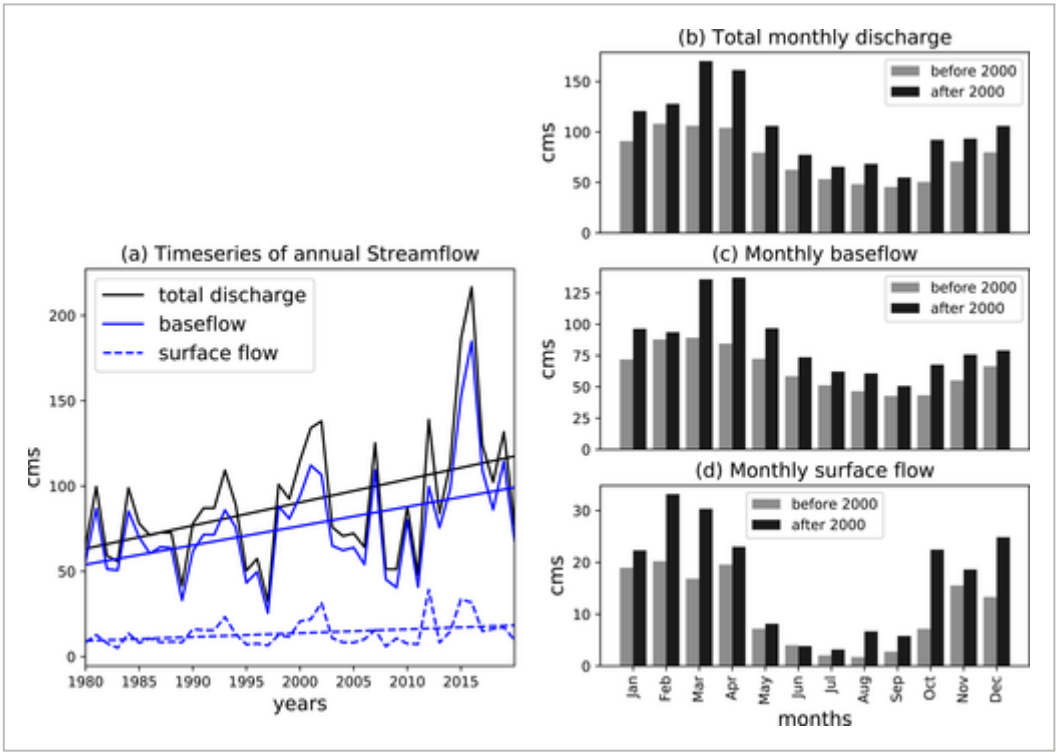

Figure 4

Open in figure viewer | PowerPoint

(a) Annual mean streamflow at Andino 1980–2016. Linear fit lines (solid straight lines) are also included. Monthly mean streamflow before and after 2000 separated into (b) total, (c) baseflow, and (d) surface flow. cms = cubic meter per second.

3.2 Effect of Changing Climate

The comparison of slopes of AET_{wb} and AET_{clim}s (calculated using Budyko framework, Section 2.2) reveals that the changes in AET cannot be fully explained by climate change alone (Figure S6 in Supporting Information S1). Slope of AET_{clim}s is positive, indicating a possible increase in AET due to climate (attributable to increasing temperature and decreasing precipitation). On the other hand, slope of AET_{wb} is negative, indicating a decrease in ET due to changed land use. The opposite trends indicate a strong dominating effect of land-use change. The equations used here are empirical and general, however, it gives us further motivation to isolate the impact of land-use change on the changes in ET and runoff trends.

3.3 Analysis of the RELAMPAGO Data

The analysis of the RELAMPAGO flux tower data is limited to the period June 1, 2018 to April 1, 2019 which corresponds to the EHOP. Figure 5 presents values at (a, d) sub-daily, (b, e) daily, and (c, f) monthly timescale. Hourly fluxes of sensible and latent heat in the soy and the alfalfa site show different characteristics. Diurnal cycles of LHF and SHF at both sites peak around 16 UTC (1 p.m. local time, Figures 5a and 5d). The difference between soy and alfalfa is largest during the daytime. The largest differences in LHF are found in November and December, while largest SHF are in October. LHF was higher for alfalfa during most of the year, except for January, February, and March, which corresponds to the peak of the soy growing season when the annual crops are transpiring vigorously (Figures 5b and 5e). SHF was higher for soy in all months, except February (Figure 5e). LHF for alfalfa (soy) peaks in December (January). SHF for alfalfa (soy) peaks in February (December). This is related to the phenology of crops in this region (see Section 2.3 and Figures S3b and S3c in Supporting Information S1). Crops transpire most during the end of growing season when they are mature. At the beginning of growing season, sensible heat is maximized. Based on our EC measurements, the accumulated 10-month ET of soy was found to be approximately 550 mm while for alfalfa it was around 880 mm.

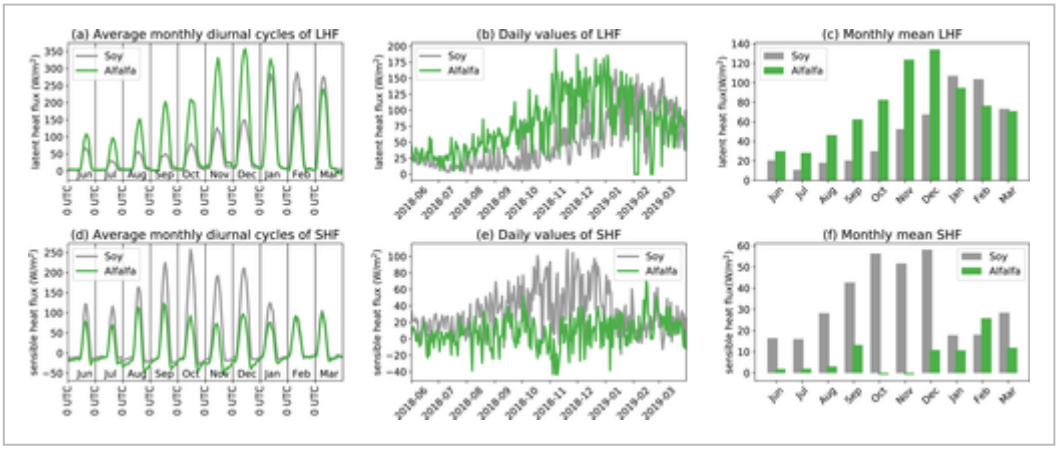

Figure 5

Open in figure viewer | PowerPoint

Diurnal, daily, and monthly values of latent (a, b, and c) and sensible heat flux (d, e, and f), respectively, at Marcos Juarez as observed by EOL towers during RELAMPAGO.

In addition to sensible and latent heat, we analyzed SH, OSR, ST, T2m, U-momentum and V-momentum, and ISR measurements from the two sites. SH is higher at the Alfalfa site in all months except February and March (Figures 6a–6c). The difference is largest in January. This indicates that the atmosphere above alfalfa is more humid due to higher transpiration of the plants. OSR is higher at the soy site in all months (Figures 6d–6f). This is likely related to higher albedo of soy when compared to Alfalfa. This radiative effect alters the net incoming solar radiation. ST is higher at the soy site in all months, except January and February (Figures 6g–6i). No significant difference was found for T2m, U-momentum and V-momentum, and ISR (not shown). This indicates that thermodynamic properties are altered by the change in vegetation, but not the dynamic properties.

Figure 6

Open in figure viewer | PowerPoint

Diurnal, daily, and monthly values of specific humidity (a, b, and c), outgoing shortwave radiation (d, e, and f), and soil temperature (g, h, and i), respectively, at Marcos Juarez as observed by EOL towers during RELAMPAGO.

WT is shallower at the soy site (Figure 7) by more than 1 m and this difference increases in summer months when we see a sharp increase in WT following the first rains (November–February). We also see that the automated WT depth measurements (continuous line) agree with the manual observations (points).

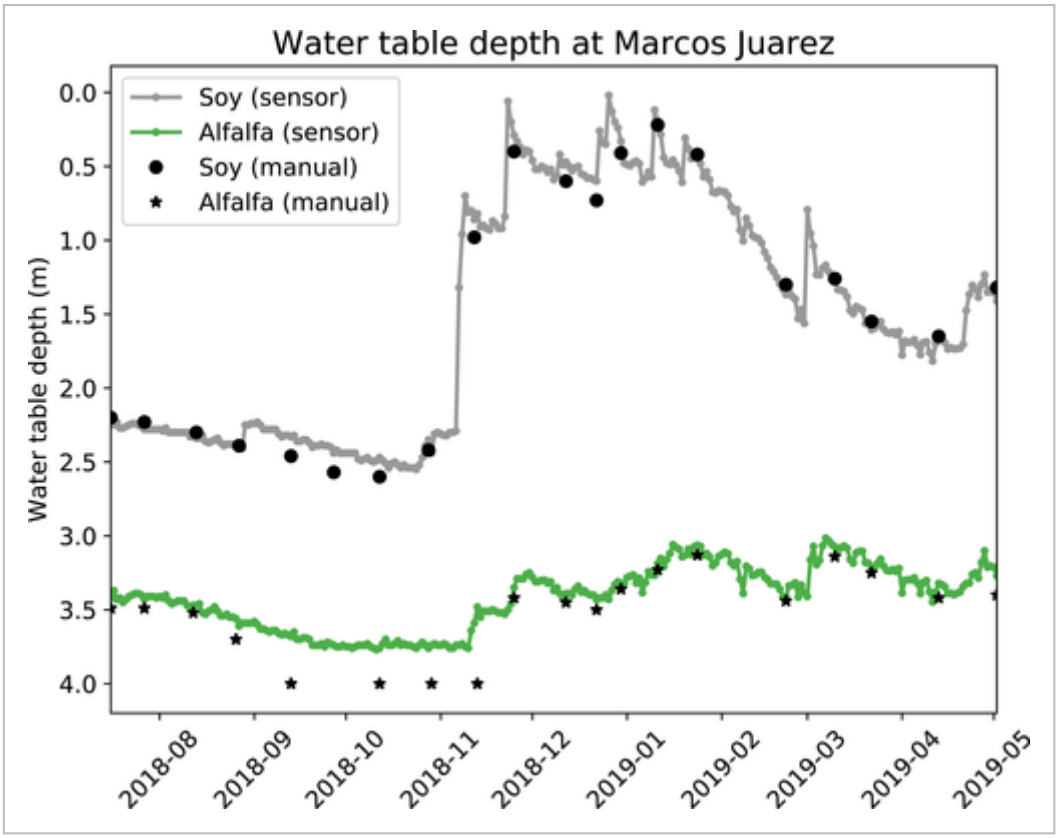

Figure 7

Open in figure viewer | PowerPoint

Water table depth at Marcos Juarez as measured by INTA during RELAMPAGO period.

3.4 Model Validation

The results of calibration and validation are shown in Table 2. For the soy (alfalfa) site, the parameters found were: VMAX = 132.425 (136.734), BP = 1,580.63 (2,041), MP = 6.89 (5.95). These values are physically realistic for C3 type vegetations (Kattge et al., 2009; Miner et al., 2017). The model performance was validated against SHF and SM, at daily scale, at both sites. The performance was significantly improved from the default parameter combinations (see Figure S7 in Supporting Information S1). Relatively better performance at the alfalfa site is likely related to the longer period of active vegetation used to calibrate parameters compared to fewer months of active vegetation at the soy site. These calibrated parameters were used in the long-term simulations Noah-MP ALFALFA LT and Noah-MP SOY LT.

Table 2. Calibration and Validation of Noah-MP at Daily Scale (304 days) at Each Site

		Alfalfa site		Soy site	
		CC	RMSE (W/m^2)	CC	RMSE(W/m^2)
Calibration	Latent heat flux	0.78	32.61	0.65	37.45

		Alfalfa site		Soy site	
		CC	RMSE (W/m^2)	CC	RMSE(W/m^2)
Validation	Sensible heat flux	0.62	24.62	0.64	20.1
	Top layer soil moisture	0.57	17.56	0.49	17.74

Note. CC, correlation coefficient, RMSE, root mean square error.

When compared to observations, the Noah-MP calibrated model performs realistically for both sites (Figure 8). The model was calibrated for daily LHF and validated with SHF and SM at the same locations. LHF at the soy site was well represented by the model, except for some high daily values in October and December (Figure 8a). LHF at the alfalfa site was slightly underestimated during some days in the Spring and overestimated in the Summer months (Figure 8b). SHF was slightly underestimated by Noah-MP at the soy site and overestimated at the alfalfa site (Figures 8c and 8d). The model does a reasonable job (Figures 8e and 8f) in simulating the top layer SM (0–5 cm), unfortunately, we do not have SM observations until November of 2018. The discrepancies between model simulated fluxes and observations can be attributed to the simple structure of the Noah-MP model and calibration of limited variables within the model. Noah-MP assumes uniform soil with depth, and uniform root distribution throughout the soil layers. However, for the purposes of this study, we are interested in comparing the representation of the two different vegetation types to understand the long-term effect of such changes in the fluxes of energy and moisture. Also, realistic land surface modeling complements the observations in terms of gap filling of missing values, which are common in these types of measurements.

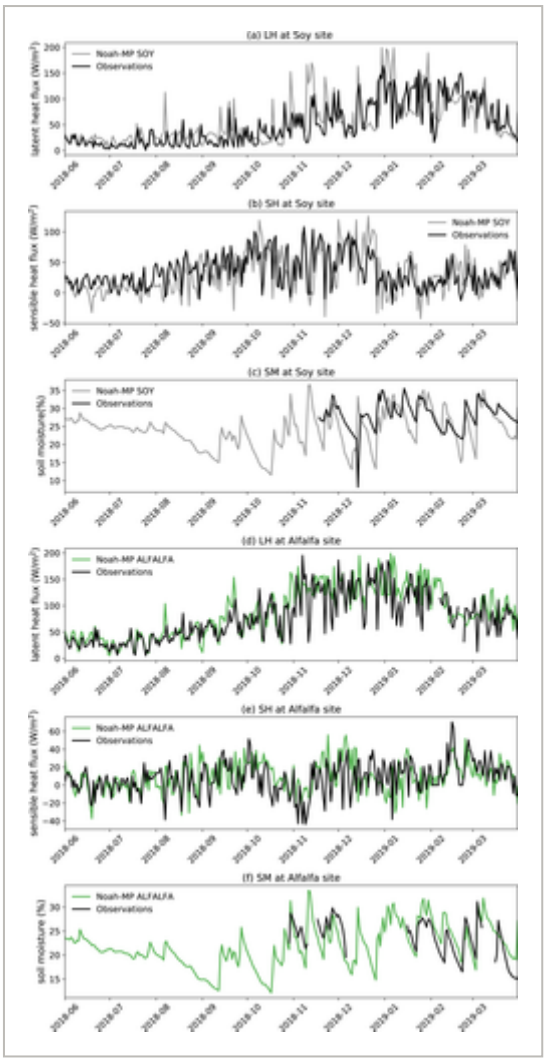

Figure 8

Open in figure viewer | PowerPoint

Calibrated Noah-MP model output at soy (a, b, and c) and alfalfa site (d, e, and f) as compared with EOL flux tower observation during RELAMPAGO period. Missing/unusual soil moisture data is omitted from the plots.

3.5 Long-Term Water and Energy Balance of the Two Experiments

To understand how changes in agricultural practices might have changed the fluxes of water and energy, we performed two idealized long-term Noah-MP simulations for the period 1970–2018. In one simulation we set the land cover as soy (Noah-MP SOY LT, Table 1), while in the other simulation was alfalfa (Noah-MP ALFALFA LT, Table 1). Both simulations have the same atmospheric forcing for the 49-year period. The annual mean values of different components of the water budget (P = ET + R + SR, where P = precipitation, ET = evapotranspiration, R = Recharge, SR = surface runoff, ignoring storage) of the two simulations are shown in Figure 9.

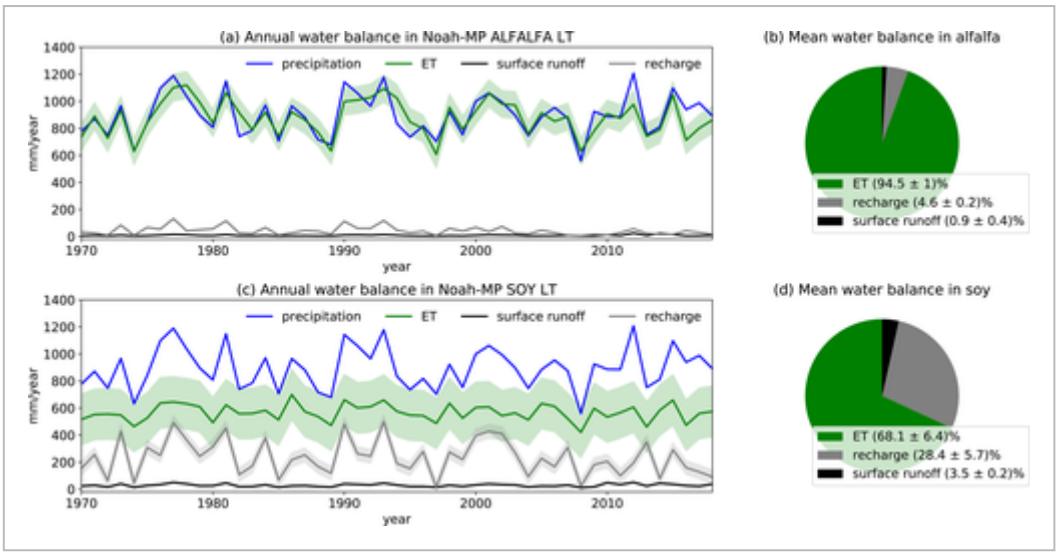

Figure 9

Open in figure viewer | PowerPoint

Long-term annual estimates of precipitation, ET, runoff, and recharge in (a) 100% alfalfa and (c) 100% soy simulations. Average partitioning of water in (b) alfalfa and (d) soy as calculated over the period 1970–2018. Shaded regions indicate the uncertainty bound.

At the alfalfa site, long-term average water balance reveals that ET is the dominant component (Figure 9a). Most of the incoming precipitation is evaporated (94.5 ± 1%) while a relatively small amount goes into the aquifer as recharge (4.6 ± 0.2%), along with negligible surface runoff (0.9 ± 0.4%). This kind of partitioning of precipitation is realistic in this region (Giménez et al., 2020; Rodriguez et al., 2020). This is due to high evaporative potential of alfalfa, adequate water availability, and flatness of the region which results in very little surface runoff. At the soy site (Figure 9b), a significant amount of precipitated water goes into the aquifer as recharge (28.4 ± 5.7%), with significantly less evaporation (68.1 ± 6.4%), when compared to alfalfa. The surface runoff component at the soy site is slightly higher (3.5 ± 0.2%), but still negligible compared to the evaporation and recharge.

Hence, changing alfalfa to soy results in a fourfold increase in runoff and a sixfold increase in deep recharge. These results are consistent with previous literature and observations (Nosetto et al., 2015; Rodriguez et al., 2020). The change in land use in this region results in more recharge, which contributes to a shallower WT depth and higher baseflow (as seen in Figures 3 and 4). In other words, the moisture that would have entered the atmosphere in alfalfa vegetated region, is being accumulated below ground due to the shift in land use to soy. This shift in regime transforms the subsurface hydrology in terms of WT depth, baseflow, and SM. Analyzing the partitioning of available energy (defined as the summation of LHF and SHF [Shuttleworth, 1993]), we find that the balance is significantly different when comparing alfalfa and soy (Figure 10). LHF accounts for 74.8 ± 2.2% of available energy over alfalfa while it accounts for 59.5 ± 2.7% over soy. On the other hand, 25.2 ± 2.2% of the available energy over alfalfa goes into SHF, while it is 40.5 ± 2.7% over soy. The Bowen ratio ($\mathrm{SHF/LHF}$) reiterates this fact, with mean of 0.2 over alfalfa and 0.7 over soy. This could also

have a potential impact on the overlying atmosphere, given this region is characterized by strong land-atmosphere coupling (Ruscica et al., 2015). It is also seen that the uncertainties in the SOY simulations are higher than ALFALFA simulations. Extra uncertainty comes from the unknown LAI estimates during the months of May to October where approximations due to cover crops were considered.

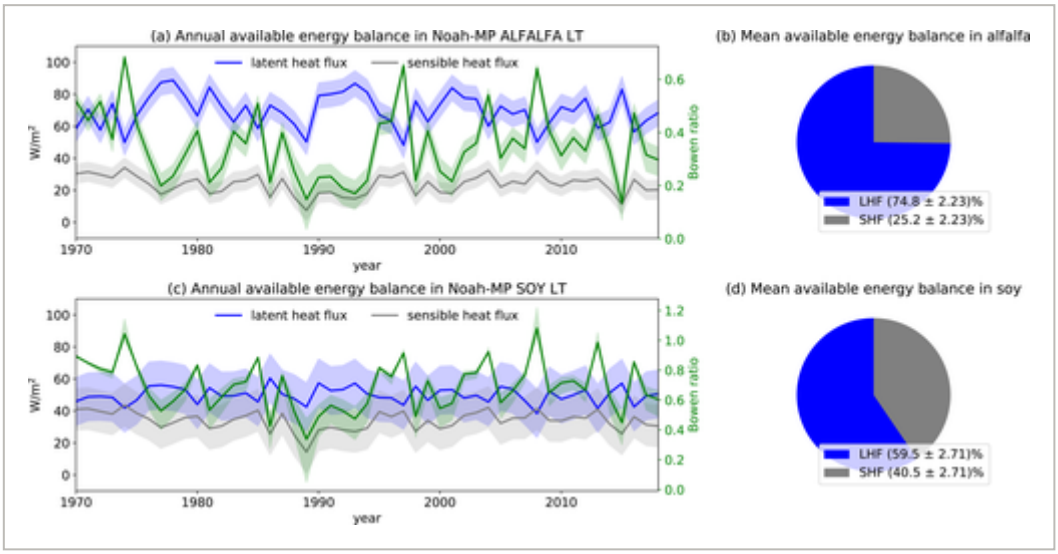

Figure 10

Open in figure viewer | PowerPoint

Long-term annual estimates of LHF and SHF in (a) 100% alfalfa and (c) 100% soy simulations. Bowen ratio is shown with green line (secondary axis). Average partitioning of available energy in (b) alfalfa and (d) soy as calculated over the period 1970–2018. Shaded regions indicate the uncertainty bound.

3.6 Idealized Transient Land Cover Analysis

In the previous section, 100% soy and 100% alfalfa idealized simulations were used to estimate long-term water and energy balance. To estimate the effect of a gradual shift in land cover (as in Figure 2) we used the weighted tile approach described in Section 2.4.3. Figures 11a–11d reveal that a gradual land-use change pattern from alfalfa to soy, results in decreased LHF and increase SHF. Similarly, annual recharge and runoff increase over time. Our results indicate a decreasing trend of ET, increasing trend of SHF, increasing trend of annual recharge (not statistically significant), and increasing trend of surface runoff (not statistically significant). Nonetheless, these long-term trends agree in sign with the observations. Increased recharge and runoff are reflected in increased baseflow and surface flow of Carcarañá river (Figure 4). Along with decreasing WT depth, this poses a higher flooding risk in the region in recent years, which is reported in many studies (Aragón et al., 2010; Nosetto et al., 2012).

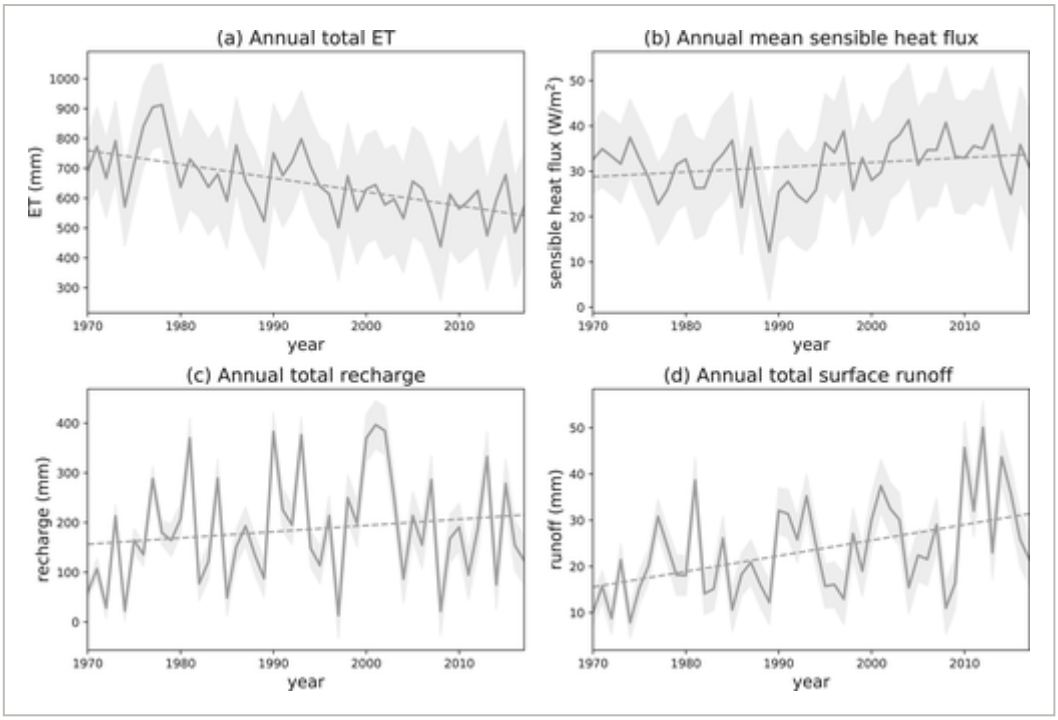

Figure 11

Open in figure viewer | PowerPoint

Long-term estimates of annual mean (a) latent heat flux, (b) sensible heat flux (c) recharge, and (d) runoff according to the land-use estimates of Figure 2. The dashed lines show the linear trends. Decreasing trend of ET was found statistically significant at 95% ($p = 6.6 \times 10^{-6}$), increasing trend of SHF was found statistically significant at 95% ($p = 2.07 \times 10^{-5}$), increasing trend of annual recharge was not found statistically significant at 95% ($p = 0.2665$), increasing trend of surface runoff was not found statistically significant at 95% ($p = 0.0016$). Shaded regions indicate the uncertainty bound.

Finally, we argue that the change in WT depth over the years is partially linked to the transient recharge estimates. It is important to highlight that we are not directly simulating absolute values of WT depth because we lack information about the specific yield of the unconfined aquifer and because we cannot simulate lateral groundwater flow in the one-column Noah-MP configuration (Niu et al., 2007). Due to these uncertainties in the groundwater scheme, we can only infer how changes in the WT depth could be related to changes in recharge. We see a slight increase (not statistically significant) in annual recharge throughout the period (Figures 11c), and therefore, the simulated trend in recharge would not solely account for the 10 m decrease in WT depth found in observations (Figure 3a). However, we find significant temporal correlation ($R = 0.54$) between interannual changes in observed WT depth change and simulated transient recharge (Figure 12). This indicates that changes in recharge driven primarily by climate variability as represented by Noah-MP, correlate well with WT depth observations. This result agrees with Mercau et al. (2015) who related annual changes in WT depth to annual balance between precipitation and evaporation (P-E). However, these magnitudes of the changes are also controlled by the type of vegetation. Figure 13 presents the change in WT depth (and recharge) as a function of

precipitation from the simulations using soy (gray dots) and alfalfa (green dots). For a given amount of precipitation, the change in WTD is higher for soy. This is particularly high in the El Niño years denoted by blue circles, when precipitation is higher than normal in southeastern South America (Cai et al., 2020). While alfalfa can still use most of the excess water as ET, land planted with soy experiences comparatively larger changes in WT depth due to higher recharge (Figure 13). This results in a difference of as large as 1 m between these two vegetation types. During drier La Niña years, denoted by red circles, precipitation is below normal in southeastern South America and vegetation has less impact on WT depth change. Hence, we conclude that interannual variability in recharge, and groundwater table depth are partially controlled by interannual climate variability and partially controlled by vegetation type. As such, the probability of large changes in WT depth during ENSO events is exacerbated when the land cover is switched from alfalfa to soy.

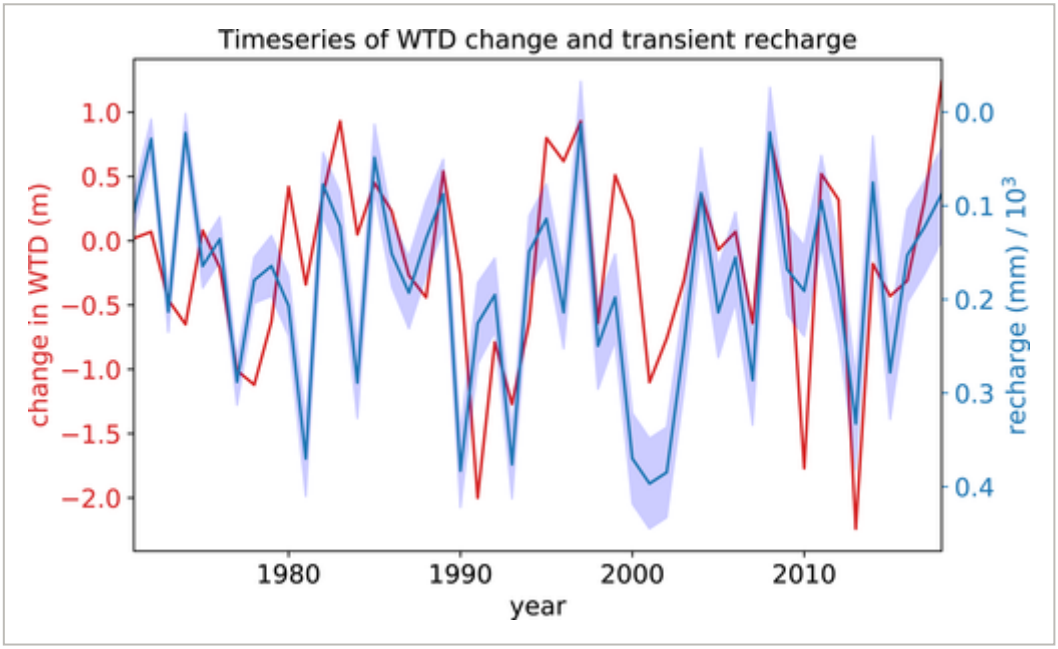

Figure 12

Open in figure viewer | PowerPoint

Timeseries of transient Noah-MP recharge and observed inter-annual variation in water table depth.

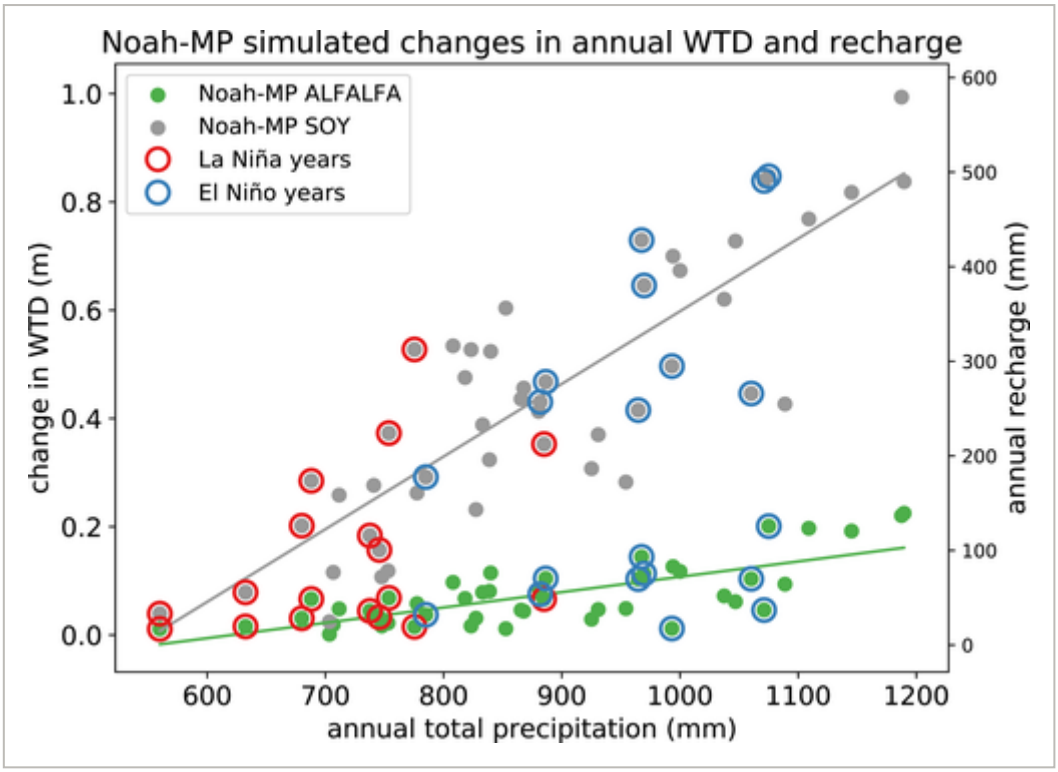

Figure 13

Open in figure viewer | PowerPoint

Effect of vegetation on the changes in WTD in different climatic years as simulated by Noah-MP. El Niño and La Niña years were identified based on Oceanic Niño Index (https://ggweather.com/enso/oni.htm). The solid lines show the linear trends in the data.

It is important to highlight that our experimental setup is highly simplified, with predefined LAI and root depth values and only one crop type in each simulation. More realistic estimates would require flux tower observations over other types of crops such as winter wheat and corn. These additional land cover types likely have the characteristics of moisture and energy fluxes in-between the soy and alfalfa. Furthermore, we do not explicitly simulate WT depth due to the fact that the one-dimensional model does not account for lateral groundwater flow and unknown aquifer-related data. However, these results show that, given identical climate conditions, the different land covers result in a very different partitioning of precipitation. Higher recharge in the soy scenario contributes to higher WT depth and more runoff.

4 Conclusions

In the past decades, there has been a dramatic shift of land cover in central Argentina from perennial to annual crops. In this study, we use detailed observations and modeling to understand how the shift in land cover has also affected the sub-surface, surface, and atmospheric fluxes of moisture and energy. Long-term observations have shown that, despite slightly decreasing precipitation, streamflow in the region has increased primarily due to baseflow. In addition, WT depth has decreased significantly since the 1970s. We

obtained data from a paired eddy-covariance tower site over alfalfa and soy crops in Marcos Juarez, Argentina as part of the RELAMPAGO field campaign. The alfalfa experimental site reflects conditions similar to those that prevailed in the 1970s, while the soy site is characteristic of the land cover of today.

Our observations reveal that ET and SH are higher at the alfalfa site, particularly for the period of July–December. The alfalfa site also has deeper WT depth. On the other hand, sensible heat, OSR, and ST are higher at the soy site. The higher sensible heat in the soy crop between June and December is particularly striking. No significant differences were found in the other variables such as T2m, U-momentum and V-momentum, and ISR. These observations were also used to calibrate Noah-MP land surface model parameters for this region.

Long-term Noah-MP simulations reveal that different land-surface properties affect the partitioning of rainfall between ET, recharge, and runoff. ET is significantly higher for alfalfa. Long-term simulations reveal that ~95% of precipitation is evaporated in the alfalfa site with negligible recharge and runoff. On the other hand, ET in the soy site accounts for ~68% of precipitation. The recharge significantly increases in case of soy (~28% from ~5% in alfalfa). Runoff also increases from 0.9% in alfalfa to 3.5% in soy. Significantly higher recharge in soy would result in higher baseflow and shallower WT, as we have seen in the observations. The effect on WT depth is even more pronounced in El Niño years when higher than normal precipitation is available, and the soy scenario shows more significant changes in WT depth than the alfalfa scenario. However, the simulated increase in recharge in the transient simulation is not totally able to account for the dramatic observed long-term change in WT depth.

Our results suggest that the large-scale changes in land cover in Argentina have likely affected sub-surface, surface, and atmospheric fluxes of moisture and energy. When compared to perennial land cover, annual crops such as soy result in a shallower and more variable WT, increased runoff driven by baseflow increases, decreased ET, and increased sensible heat. In other words, much of the water that was going into the atmosphere in the 1970s is now going into the surface and subsurface. Furthermore, the energy that was being used to evaporate the water is now going into sensible heat, and this results in a dramatic 250% increase in the Bowen ratio. The implications of this shift in fluxes of moisture and energy to the weather and climate will be the focus of future work, using a regional Noah-MP “coupled” to the atmosphere. The regional coupled framework will allow us to better represent the lateral fluxes and evaluate the feedbacks between the atmosphere and land fluxes which were not included in the present study.

Acknowledgments

Support for this study has been provided by the National Science Foundation (NSF) Grant 1641167 “RELAMPAGO Hydrometeorology Component: Land Surface Controls on Heavy

Precipitation and Flooding in the Carcarañá River Basin, Argentina." Additional funding for Sujan Pal was provided by NSF CAREER Award (PI – Francina Dominguez) AGS 1454089 "Hydroclimatic Response to Natural and Anthropogenic Land Cover Change over South America: A Focus on the La Plata River Basin".

Conflict of Interest

The authors declare no conflicts of interest relevant to this study.

Open Research

Data Availability Statement

The observed data sets, model inputs, and model setup are stored at the Zenodo repository (doi: 10.5281/zenodo.5128498). The authors acknowledge NCAR EOL team for collection, quality control, and storage of RELAMPAGO data.

Supporting Information

Filename	Description
2021WR029704-sup-0001-Supporting Information SI-S01.docx 899.5 KB	Supporting Information S1

Please note: The publisher is not responsible for the content or functionality of any supporting information supplied by the authors. Any queries (other than missing content) should be directed to the corresponding author for the article.

References

Aragón, R., Jobbágy, E. G., & Viglizzo, E. F. (2010). Surface and groundwater dynamics in the sedimentary plains of the Western Pampas (Argentina). *Ecohydrology*, **4**(3), 433– 447. https://doi.org/10.1002/eco.149
Wiley Online Library | Web of Science® | Google Scholar

Baldi, G., & Paruelo, J. M. (2008). Land-use and land cover dynamics in South American temperate grasslands Ecol. *Forestry and Society*, **13**, 6. https://doi.org/10.5751/es-02481-130206
Google Scholar

Ball, J. T., Woodrow, I. E., & Berry, J. A. (1987). A model predicting stomatal conductance and its contribution to the control of photosynthesis under different environmental conditions. In *Progress in photosynthesis research* (pp. 221– 224). Springer Netherlands. https://doi.org/10.1007/978-94-017-0519-6_48
Crossref | Web of Science® | Google Scholar

Budyko, M. I. (1974). *Climate and life* (p. 508). Academic Press.
Google Scholar

Cai, W., McPhaden, M. J., Grimm, A. M., Rodrigues, R. R., Taschetto, A. S., Garreaud, R. D., et al. (2020). Climate impacts of the El Niño–Southern Oscillation on South America. *Nature Reviews Earth & Environment*, **1**, 215– 231. https://doi.org/10.1038/s43017-020-0040-3
Crossref | ADS | Google Scholar

Chen, F., & Dudhia, J. (2001). Coupling an advanced land surface-hydrology model with the Penn State-NCAR MM5 modeling system. Part I: Model implementation and sensitivity. *Monthly Weather Review*, **129**(4), 569– 585. https://doi.org/10.1175/1520-0493(2001)129<0569:caalsh>2.0.co;2
Crossref | ADS | Web of Science® | Google Scholar

Cuntz, M., Mai, J., Samaniego, L., Clark, M., Wulfmeyer, V., Branch, O., et al. (2016). The impact of standard andhard-coded parameters on the hydrologic fluxes in the Noah-MPland surface model. *Journal of Geophysical Research - D: Atmospheres*, **121**(18), 10676– 10700. https://doi.org/10.1002/2016JD025097
Wiley Online Library | ADS | Web of Science® | Google Scholar

Duan, Q., Gupta, V. K., & Sorooshian, S. (1993). Shuffled complex evolution approach for effective and efficient global minimization. *Journal of Optimization Theory and Applications*, **76**(3), 501– 521. https://doi.org/10.1007/bf00939380
Crossref | Web of Science® | Google Scholar

Eckhardt, K. (2012). Technical note: Analytical sensitivity analysis of a two parameter recursive digital baseflow separation filter. *Hydrology and Earth System Sciences*, **16**, 451– 455. https://doi.org/10.5194/hess-16-451-2012
Crossref | ADS | Web of Science® | Google Scholar

Farquhar, G. D., von Caemmerer, S., & Berry, J. A. (1980). A biochemical model of photosynthetic CO_2 assimilation in leaves of C_3 species. *Planta*, **149**, 78– 90. https://doi.org/10.1007/BF00386231
Crossref | CAS | PubMed | Web of Science® | Google Scholar

García, A. G., Di Bella, C. M., Houspanossian, J., Magliano, P. N., Jobbágy, E. G., Posse, G., et al. (2017). Patterns and controls of carbon dioxide and water vapor fluxes in a dry forest of Central Argentina. *Agricultural and Forest Meteorology*, **247**, 520– 532. https://doi.org/10.1016/j.agrformet.2017.08.015
Crossref | ADS | Web of Science® | Google Scholar

García, P. E., Menénendez, A. N., Podestá, G., Bert, F., Arora, P., & Jobbágy, E. (2017). Land use as possible strategy for managing water table depth in flat basins with shallow groundwater. *International Journal of River Basin Management*, **16**(1), 79– 92.
https://doi.org/10.1080/15715124.2017.1378223
Crossref | Web of Science® | Google Scholar

Giménez, R., Mercau, J. L., Bert, F. E., Kuppel, S., Baldi, G., Houspanossian, J., et al. (2020). Hydrological and productive impacts of recent land-use and land-cover changes in the semiarid Chaco: Understanding novel water excess in water scarce farmlands. *Ecohydrology*, **13**, e2243.
https://doi.org/10.1002/eco.2243
Wiley Online Library | Web of Science® | Google Scholar

Graesser, J., Aide, T. M., Grau, H. R., & Ramankutty, N. (2015). Cropland/pastureland dynamics and the slowdown of deforestation in Latin America. *Environmental Research Letters*, **10**(3), 034017.
https://doi.org/10.1088/1748-9326/10/3/034017
Crossref | Web of Science® | Google Scholar

Houska, T., Kraft, P., Chamorro-Chavez, A., & Breuer, L. (2015). SPOTting model parameters using a ready-made python package. *PLOS One*, **10**(12), e0145180.
https://doi.org/10.1371/journal.pone.0145180
Crossref | PubMed | Web of Science® | Google Scholar

Jaramillo, F., Prieto, C., Lyon, S. W., & Destouni, G. (2013). Multimethod assessment of evapotranspiration shifts due to non-irrigated agricultural development in Sweden. *Journal of Hydrology*, **484**, 55– 62. https://doi.org/10.1016/j.jhydrol.2013.01.010
Crossref | ADS | Web of Science® | Google Scholar

Jobbagy, G. E. G., Nosetto, M. D., ssantoni, C. S., & Baldi, G. (2008). El desafío ecohidrológico de las transiciones entre sistemas leñosos y herbáceos en la llanura Chaco-Pampeana. *Ecologia Austral*, **18**, 305– 322.
Google Scholar

Jobbágy, G. E. G., Santiago, L., Ricardo, P., Buono, N. S., Yésica, D., Marchesini, V., & Nosetto, M. (2020). Plants vs. Streams: Their groundwater-mediated competition at “El Morro”, a developing catchment in the dry plains of Argentina. *Authorea*.
https://doi.org/10.22541/au.160133536.67833093
Google Scholar

Kattge, J., Knorr, W., Raddatz, T., & Wirth, C. (2009). Quantifying photosynthetic capacity and its relationship to leaf nitrogen content for global-scale terrestrial biosphere models. *Global Change Biology*, **15**, 976– 991. https://doi.org/10.1111/j.1365-2486.2008.01744.x
Wiley Online Library | ADS | Web of Science® | Google Scholar

Kljun, N., Calanca, P., Rotach, M. W., & Schmid, H. P. (2015). A simple two-dimensional parameterisation for Flux Footprint Prediction (FFP), Geosci. *Model Development*, **8**, 3695– 3713.
https://doi.org/10.5194/gmd-8-3695-2015

Crossref | ADS | Web of Science® | Google Scholar

Kuppel, S., Houspanossian, J., Nosetto, M. D., & Jobbágy, E. G. (2015). What does it take to flood the Pampas? Lessons from a decade of strong hydrological fluctuations. *Water Resources Research*, **51**(4), 2937– 2950. https://doi.org/10.1002/2015WR016966
Wiley Online Library | ADS | Web of Science® | Google Scholar

Langbein, W. B. (1949). Annual runoff in the United States (Vol. **52**, p. 14). US Geological Survey Circular.
Google Scholar

Lee, E., Livino, A., Han, SC., Zhang, K., Briscoe, J., Kelman, J., & Moorcroft, P. (2018). Land cover change explains the increasing discharge of the Paraná River. *Regional Environmental Change*, **18**, 1871– 1881. https://doi.org/10.1007/s10113-018-1321-y
Crossref | PubMed | Web of Science® | Google Scholar

Levi, L., Jaramillo, F., Andričević, R., & Destouni, G. (2015). Hydroclimatic changes and drivers in the Sava River Catchment and comparison with Swedish catchments. *Ambio*, **44**, 624– 634. https://doi.org/10.1007/s13280-015-0641-0
Crossref | CAS | PubMed | Web of Science® | Google Scholar

Martinez, J. A., Dominguez, F., & Miguez-Macho, G. (2016a). Effects of a groundwater scheme on the simulation of soil moisture andevapotranspiration over southern South America. *Journal of Hydrometeorology*, **17**, 2941– 2957. https://doi.org/10.1175/JHM-D-16-0051.1
Crossref | ADS | Web of Science® | Google Scholar

Martinez, J. A., Dominguez, F., & Miguez-Macho, G. (2016b). Impacts of a groundwater scheme on hydroclimatological conditions over southern South America. *Journal of Hydrometeorology*, **17**, 2959– 2978. https://doi.org/10.1175/JHM-D-16-0052.1
Crossref | ADS | Web of Science® | Google Scholar

Mercau, J. L., Nosetto, M. D., Bert, F., Giménez, R., & Jobbágy, E. G. (2015). Shallow groundwater dynamics in the Pampas: Climate, landscape and crop choice effects. *Agricultural Water Management*, **163**, 159– 168. https://doi.org/10.1016/j.agwat.2015.09.013
Crossref | Web of Science® | Google Scholar

Miguez-Macho, G., & Fan, Y. (2012). The role of groundwater in the Amazon water cycle: 1. Influence on seasonal streamflow, flooding and wetlands. *Journal of Geophysical Research*, **117**, D15113. https://doi.org/10.1029/2012JD017539
Web of Science® | Google Scholar

Miner, G. L., Bauerle, W. L., & Baldocchi, D. D. (2017). Estimating the sensitivity of stomatal conductance to photosynthesis: A review. *Plant, Cell and Environment*, **40**, 1214– 1238. https://doi.org/10.1111/pce.12871
Wiley Online Library | CAS | PubMed | Web of Science® | Google Scholar

Modarres, R., & Sarhadi, A. (2009). Rainfall trends analysis of Iran in the last half of the twentieth century. *Journal of Geophysical Research: Atmospheres*, **114**, D03101. https://doi.org/10.1029/2008jd010707
Wiley Online Library | ADS | Web of Science® | Google Scholar

Nesbitt, S. W., Roberts, R., Trapp, J., Dominguez, F., & Gochis, D. (2016). *RELAMPAGO experimental design overview*. Retrieved from https://www.eol.ucar.edu/field_projects/relampago
Google Scholar

Niu, G.-Y., Yang, Z. -L., Dickinson, R. E., Gulden, L. E., & Su, H. (2007). Development of a simple groundwater model for use in climate models and evaluation with gravity recovery and climate experiment data. *Journal of Geophysical Research*, **112**, D07103. https://doi.org/10.1029/2006JD007522
Wiley Online Library | ADS | Web of Science® | Google Scholar

Niu, G.-Y., Yang, Z.-L., Mitchell, K. E., Chen, F., Ek, M. B., Barlage, M., et al. (2011). The Community Noah Land Surface Model withMulti-Parameterization Options (NOAH-MP): 1. Model description and evaluation with local-scale measurements. *Journal of Geophysical Research*, **116**, D12109. https://doi.org/10.1029/2010JD015139
Wiley Online Library | ADS | Web of Science® | Google Scholar

Nosetto, M. D., Jobbágy, E. G., Brizuela, A. B., & Jackson, R. B. (2012). The hydrologic consequences of land cover change in central Argentina. *Agriculture, Ecosystems & Environment*, **154**, 2– 11. https://doi.org/10.1016/j.agee.2011.01.008
Crossref | Web of Science® | Google Scholar

Nosetto, M. D., Luna Toledo, E., Magliano, P. N., Figuerola, P., Blanco, L. J., & Jobbágy, E. G. (2020). Contrasting CO_2 and water vapour fluxes in dry forest and pasture sites of central Argentina. *Ecohydrology*, **13**, e2244. https://doi.org/10.1002/eco.2244
Wiley Online Library | CAS | Web of Science® | Google Scholar

Nosetto, M. D., Paez, R. A., Ballesteros, S. I., & Jobbágy, E. G. (2015). Higher water-table levels and flooding risk under grain vs. livestock production systems in the subhumid plains of the Pampas. *Agriculture, Ecosystems & Environment*, **206**, 60– 70. https://doi.org/10.1016/j.agee.2015.03.009
Crossref | Web of Science® | Google Scholar

Oncley, S. P., Foken, T., Vogt, R., Kohsiek, W., DeBruin, H. A. R., Bernhofer, C., et al. (2007). The energy balance experiment EBEX-2000. Part I: Overview and energy balance. *Boundary-Layer Meteorology*, **123**, 1– 28. https://doi.org/10.1007/s10546-007-9161-1
Crossref | ADS | Web of Science® | Google Scholar

Pal, S., Dominguez, F., Dillon, M. E., Alvarez, J., Garcia, C. M., Nesbitt, S. W., & Gochis, D. (2021). Hydrometeorological observations and modeling of an extreme rainfall event using WRF and WRF-Hydro during the RELAMPAGO field campaign in Argentina, *Journal of Hydrometeorology*, **22**(2), 331– 351. https://doi.org/10.1175/JHM-D-20-0133.1
Crossref | ADS | Web of Science® | Google Scholar

Paruelo, J. M., Guerschman, J. P., & Veron, S. R. (2005). Expansion Agricola y cambios en el uso del suelo. *Ciencia Hoy*, **1–10**.
Google Scholar

Rodell, M., Houser, P. R., Jambor, U., Gottschalck, J., Mitchell, K., Meng, C.-J., et al. (2004). The global land data assimilation system. *Bulletin of the American Meteorological Society*, **85**, 381– 394. https://doi.org/10.1175/BAMS-85-3-381
Crossref | ADS | Web of Science® | Google Scholar

Rodriguez, P., Giménez, R., Nosetto, M. D., Jobbágy, E. G., & Magliano, P. N. (2020). Changes in water fluxes partition related to the replacement of native dry forests by crops in the Dry Chaco. *Journal of Arid Environments*, **183**, 104281. https://doi.org/10.1016/j.jaridenv.2020.104281
Crossref | ADS | Web of Science® | Google Scholar

Ruscica, R. C., Sörensson, A. A., Menéndez, C. G. (2015). Pathways between soil moisture and precipitation in southeastern South America. *Atmospheric Science Letters*, **16**(3), 267– 272. https://doi.org/10.1002/asl2.552
Wiley Online Library | ADS | Web of Science® | Google Scholar

Schilling, K. E., Chan, K.-S., Liu, H., & Zhang, Y.-K. (2010). Quantifying the effect of land use land cover change on increasing discharge in the Upper Mississippi River. *Journal of Hydrology*, **387**(3–4), 343– 345. https://doi.org/10.1016/j.jhydrol.2010.04.019
Crossref | ADS | Web of Science® | Google Scholar

Schilling, K. E., Jha, M. K., Zhang, Y.-K., Gassman, P. W., & Wolter, C. F. (2008). Impact of land use and land cover change on the water balance of a large agricultural watershed: Historical effects and future directions. *Water Resources Research*, **44**(7), 563– 612. https://doi.org/10.1029/2007WR006644
Wiley Online Library | Google Scholar

Sellers, P. J., Dickinson, R. E., Randall, D. A., Betts, A. K., Hall, F. G., Berry, J. A., et al. (1997). Modeling the exchanges of energy, water, and carbon between continents and the atmosphere. *Science*, **275**(5299), 502– 509. https://doi.org/10.1126/science.275.5299.502
Crossref | CAS | PubMed | Web of Science® | Google Scholar

Shuttleworth, WJ. (1993). Evaporation. In D. R. Maidment (Ed.), *Handbook of hydrology*. (pp. 4.1–4.53). McGraw-Hill, Inc.
Google Scholar

Sneyers, R. (1990). *On statistical analysis of series of observation*. Technical note No.143, WMO No. 415. World Meteorological Organization.
Google Scholar

Sörensson, A. A., & Berbery, E. H. (2015). A note on soil moisture memory and interactions with surface climate for different vegetation types in the La Plata basin. *Journal of Hydrometeorology*, **16**,

716– 729. https://doi.org/10.1175/JHM-D-14-0102.1
Crossref | ADS | Web of Science® | Google Scholar

Turc, L. (1954). The water balance of soils—Relation between precipitation evaporation and flow. *Annales Agronomiques*, **5**, 491– 569.
CAS | Google Scholar

Varni, M., Comas, R., Weinzettel, P., & Dietrich, S. (2013). Application of the water table fluctuation method to characterize groundwater recharge in the Pampa plain, Argentina. *Hydrological Sciences Journal*, **58**(7), 1445– 1455. https://doi.org/10.1080/02626667.2013.833663
Crossref | Web of Science® | Google Scholar

Viglizzo, E. F., Jobbágy, E. G., Carreño, L., Frank, F. C., Aragón, R., Oro, L. D., & Salvador, V. (2009). The dynamics of cultivation and floods in arable lands of Central Argentina. *Hydrology and Earth System Sciences*, **13**(4), 491– 502. https://doi.org/10.5194/hess-13-491-2009
Crossref | ADS | Web of Science® | Google Scholar

Xiong, M., Huang, C.-S., & Yang, T. (2020). Assessing the impacts of climate change and land use/cover change on runoff based on improved Budyko framework models considering arbitrary partition of the impacts. *Water*, **12**, 1612. https://doi.org/10.3390/w12061612
Crossref | Web of Science® | Google Scholar

Xu, X., Scanlon, B. R., Schilling, K., & Sun, A. (2013). Relative importance of climate and land surface changes on hydrologic changes in the US Midwest since the 1930s: Implications for biofuel production. *Journal of Hydrology*, **497**, 110– 120. https://doi.org/10.1016/j.jhydrol.2013.05.041
Crossref | ADS | Web of Science® | Google Scholar

Yaeger, M. A., Sivapalan, M., McIsaac, G. F., & Cai, X. (2013). Comparative analysis of hydrologic signatures in two agricultural watersheds in east-central Illinois: Legacies of the past to inform the future. *Hydrology and Earth System Sciences*, **17**(11), 4607– 4623.
https://doi.org/10.5194/hess-17-4607-2013
Crossref | ADS | Web of Science® | Google Scholar

Zellner, M., García, G. A., Bert, F., Massey, D., & Nosetto, M. (2020). Exploring reciprocal interactions between groundwater and land cover decisions in flat agricultural areas and variable climate. *Environmental Modelling & Software*, **126**, 104641.
https://doi.org/10.1016/j.envsoft.2020.104641
Crossref | Web of Science® | Google Scholar

Zhang, Y. K., & Schilling, K. E. (2006). Increasing streamflow and baseflow in Mississippi River since the 1940s: Effect of land use change. *Journal of Hydrology*, **324**(1–4), 412– 422.
https://doi.org/10.1016/j.jhydrol.2005.09.033
Crossref | ADS | Web of Science® | Google Scholar

Zheng, H., Yang, Z. L., Lin, P. R., Wei, J. F., Wu, W. Y., Li, L. C., et al. (2019). On the sensitivity of the precipitation partitioning into evapotranspiration and runoff in land surface parameterizations.

Water Resources Research, **55**, 95– 111. https://doi.org/10.1029/2017WR022236
Wiley Online Library | ADS | Web of Science® | Google Scholar

Download PDF

Back to Top